

# The dynamics of starvation and recovery

<sup>1</sup> Justin D. Yeakel \* †‡, Christopher P. Kempes †, and Sidney Redner †§

<sup>3</sup> \*School of Natural Science, University of California Merced, Merced, CA, †The Santa Fe Institute, Santa Fe, NM, §Department of Physics, Boston University, Boston  
<sup>4</sup> MA, and ‡To whom correspondence should be addressed: jdyeakel@gmail.com

<sup>5</sup> Submitted to Proceedings of the National Academy of Sciences of the United States of America

**This is the abstract. [No it isn't. It's merely a placeholder.]**

foraging | starvation | reproduction

## Introduction

The behavioral ecology of most, if not all, organisms is influenced by the energetic state of individuals, which directly influences how they invest reserves in uncertain environments. Such behaviors are generally manifested as trade-offs between investing in somatic maintenance and growth, or allocating energy towards reproduction [?, ?, ?]. The timing of these behaviors responds to selective pressure, as the choice of the investment impacts future fitness [?]. The influence of resource limitation on an organism's ability to maintain its nutritional stores may lead to repeated delays or shifts in reproduction over the course of an organism's life.

The life history of most species is typically comprised of (a) somatic growth and maintenance, and (b) reproduction. The balance between these two activities is often conditioned on resource availability [?]. For example, reindeer invest less in calves born after harsh winters (when the mother's energetic state is depleted) than in calves born after moderate winters [?]. Many bird species invest differently in broods during periods of resource scarcity compared to normal periods [?, ?], sometimes delaying or even foregoing reproduction for a breeding season [?, ?, ?]. Even freshwater and marine zooplankton have been observed to avoid reproduction under nutritional stress [?], and those that do reproduce have lower survival rates [?]. Organisms may also separate maintenance and growth from reproduction over space and time: many salmonids, birds, and some mammals return to migratory breeding grounds to reproduce after one or multiple seasons in resource-rich environments where they accumulate nutritional reserves [?, ?, ?].

Physiological mechanisms also play an important role in regulating reproductive expenditures during periods of resource limitation. The data collected thus far has shown that diverse mammals (47 species in 10 families) exhibit delayed implantation, whereby females postpone fetal development (blastocyst implantation) until times where nutritional reserves can be accumulated [?, ?]. Many other many species (including humans) suffer irregular menstrual cycling and higher spontaneous abortion rates during periods of nutritional stress [?, ?]. In the extreme case of unicellular organisms, nutrition is unavoidably linked to reproduction because the nutritional state of the cell regulates all aspects of the cell cycle [?]. The existence of so many independently evolved mechanisms across such a diverse suite of organisms highlights the importance and universality of the fundamental tradeoff between somatic and reproductive investment. However the dynamic implications of these constraints are unknown.

Though straightforward conceptually, incorporating the energetic dynamics of individuals [?] into a population-level framework [?, ?] presents numerous mathematical obstacles [?]. An alternative approach involves modeling the macroscale relations that guide somatic versus reproductive investment in a consumer-resource system. For example, macroscale Lotka-Volterra models assume that the growth rate of the consumer population depends on resource density, thus *implicitly* incor-

porating the requirement of resource availability for reproduction [?].

In this work, we adopt an alternative approach in which resource limitation and the subsequent effect of starvation is accounted for *explicitly*. Namely, only individuals with sufficient energetic reserves can reproduce. Such a constraint leads to reproductive time lags due to some members of the population going hungry and then recovering. Additionally, we incorporate the idea that reproduction is strongly constrained allometrically [?], and is not generally linearly related to resource density. As we shall show, these constraints influence the ensuing population dynamics in dramatic ways.

**74 Nutritional-state-structured model (NSM)**  
We begin by defining a minimal Nutritional-State-structured population Model (NSM), where the consumer population is divided into two energetic states: (a) an energetically replete (full) state  $F$ , where the consumer reproduces at a constant rate  $\lambda$  and has no mortality risk, and (b) an energetically deficient (hungry) state  $H$ , where the consumer does not reproduce but dies at rate  $\mu$ . The underlying resource  $R$  evolves by logistic growth with an intrinsic growth rate  $\alpha$  and a carrying capacity equal to one. Consumers transition from the full state  $F$  to the hungry state  $H$  at a rate  $\sigma$ —the starvation rate—and also in proportion to the absence of resources  $(1 - R)$ . Conversely, consumers recover from state  $H$  to state  $F$  at rate  $\rho$  and in proportion to  $R$ . Resources are also eaten by the consumers—at rate  $\rho$  by hungry consumers and at rate  $\beta < \rho$  by full consumers. This inequality accounts for hungry consumers requiring more resources to rebuild body weight.

In the mean-field approximation, in which the consumers and resources are perfectly mixed, their densities evolve according to the rate equations

$$\begin{aligned}\dot{F} &= \lambda F + \rho RH - \sigma(1 - R)F, \\ \dot{H} &= \sigma(1 - R)F - \rho RH - \mu H, \\ \dot{R} &= \alpha R(1 - R) - R(\rho H + \beta F).\end{aligned}\quad [1]$$

Notice that the total consumer density  $F + H$  evolves according to  $\dot{F} + \dot{H} = \lambda F - \mu H$ . This resembles the equation of motion for the predator density in the classic Lotka-Volterra model, except that the resource density does not appear in the growth term. As discussed above, the attributes of reproduction and mortality have been explicitly apportioned to the full and hungry consumers, respectively, so that the growth in the total density is decoupled from the resource density.

## Reserved for Publication Footnotes

103 Equation [1] has three fixed points: two trivial fixed points 161 If  $\rho$  exceeds a threshold value, cyclic dynamics will develop as  
 104 at  $(F^*, H^*, R^*) = (0, 0, 0)$  and  $(0, 0, 1)$ , and one non-trivial, 162 the Hopf bifurcation is approached.  
 105 internal fixed point at

$$F^* = \frac{\alpha\lambda\mu(\mu + \rho)}{(\lambda\rho + \mu\sigma)(\lambda\rho + \mu\beta)},$$

$$H^* = \frac{\alpha\lambda^2(\mu + \rho)}{(\lambda\rho + \mu\sigma)(\lambda\rho + \mu\beta)},$$

$$R^* = \frac{\mu(\sigma - \lambda)}{\lambda\rho + \mu\sigma}.$$

106 The stability of this fixed point is determined by the Jaco- 161  
 107 bian Matrix  $\mathbf{J}$ , where each matrix element  $J_{ij}$  equals  $\partial\dot{X}_i/\partial X_j$   
 108 when evaluated at the internal fixed point, and  $\mathbf{X}$  is the vec- 162  
 109 tor  $(F, H, R)$ . The parameters in Eq. [1] are such that the 163  
 110 real part of the largest eigenvalue of  $\mathbf{J}$  is negative, so that the 164  
 111 system is stable with respect to small perturbations from the 165  
 112 fixed point. Because this fixed point is unique, it is the global 166  
 113 attractor for all population trajectories for any initial condition 167  
 114 where the resource and consumer densities are both non zero. 168

115 From Eq. [2], an obvious constraint on the NSM is that 169  
 116 the reproduction rate  $\lambda$  must be less than the starvation rate 170  
 117  $\sigma$ , so that  $R^*$  is positive. In fact, when the resource density 171  
 118  $R = 0$ , the rate equation for  $F$  gives exponential growth of 172  
 119  $F$  for  $\lambda > \sigma$ . The condition  $\sigma = \lambda$  represents a transcritical 173  
 120 (TC) bifurcation that demarcates the physical and unphysical 174  
 121 regimes [give Ref]. The biological implication of the constraint 175  
 122  $\lambda < \sigma$  has a simple interpretation—the rate at which a macro- 176  
 123 scopic organism loses mass due to lack of resources is generally 177  
 124 much faster than the rate of reproduction. As we will discuss 178  
 125 below, this inequality is a natural consequence of allometric 179  
 126 constraints [?] for organisms within empirically observed body 180  
 127 size ranges (Fig. 2).

128 In the physical regime of  $\lambda < \sigma$ , the fixed point [2] may 181  
 129 either be a stable node or a limit cycle (Fig. 3). In continuous- 182  
 130 time systems, a limit cycle arises when a pair of complex con- 183  
 131 jugate eigenvalues crosses the imaginary axis to attain positive 184  
 132 real parts [?]. This Hopf bifurcation is defined by  $\text{Det}(\mathbf{S}) = 0$ , 185  
 133 with  $\mathbf{S}$  the Sylvester matrix, which is composed of the coef- 186  
 134 ficients of the characteristic polynomial of the Jacobian ma- 187  
 135 trix [?]. As the system parameters are tuned to be within the 188  
 136 stable regime but close to the Hopf bifurcation, the amplitude 189  
 137 of the transient but decaying cycles become large. Given that 190  
 138 ecological systems are constantly being perturbed [?], the onset 191  
 139 of transient cycles, even though they decay with time in the 192  
 140 mean-field description, can increase the extinction risk [?, ?, ?]. 193  
 141 Thus the distance of a system from the Hopf bifurcation pro- 194  
 142 vides a measure of its persistence.

143 When the starvation rate  $\sigma \gg \lambda$ , a substantial fraction 195  
 144 of the consumers are driven to the hungry non-reproducing 196  
 145 state. Because reproduction is inhibited, there is a low steady- 197  
 146 state consumer density and a high steady-state resource den- 198  
 147 sity. However, if  $\sigma/\lambda \rightarrow 1$  from above, the population is 199  
 148 overloaded with energetically-replete (reproducing) individuals, 200  
 149 thereby promoting oscillations between the consumer and re- 201  
 150 source densities (Fig. 3).

151 Whereas the relation between consumer growth rate  $\lambda$  and 202  
 152 the starvation rate  $\sigma$  defines an absolute bound of biological 203  
 153 feasibility—the TC bifurcation—the starvation rate  $\sigma$  also de- 204  
 154 termines the sensitivity of the consumer population to changes 205  
 155 in resource density. When  $\sigma \gg \lambda$ , the steady-state population 206  
 156 density is small, thereby increasing the risk of stochastic ex- 207  
 157 tinction. On the other hand, as  $\sigma$  decreases, the system will 208  
 158 ultimately be poised either near the TC or the Hopf bifurcation 209  
 159 (Fig. 3). If the recovery rate  $\rho$  is sufficiently small, the TC bi- 210  
 160 furcation is reached and the resource eventually is eliminated. 211

163 [mention and refer to the starving random walk  
 164 model somewhere.]

## 165 166 Role of allometry

167 The NSM describes a broad range of dynamics, yet organisms 168  
 169 are likely unable to access most of the total parameter space. 170  
 171 Here we use allometric scaling relations to constrain the covaria- 172  
 173 tion of rates in a principled and biologically meaningful manner. 174  
 175 Allometric scaling relations highlight common constraints and 176  
 177 average trends across large ranges in body size and species di- 178  
 179 versity. Many of these relations can be derived from a small set 180  
 181 of assumptions and below we describe a framework to deter- 182  
 183 mine the covariation of timescales and rates across the range of 184  
 185 mammals for each of the key parameters of our model (cf. [?]). 186  
 187 We are thereby able to define the regime of dynamics occupied 188  
 189 by the entire class of mammals along with the key differences 190  
 191 between the largest and smallest mammals.

192 Nearly all of the rates described in the NSM are to some 193 extent governed by consumer metabolism, which can be used to 194  
 195 describe a variety of organismal features [Ref]. The scaling 196  
 197 relation between an organism's metabolic rate  $B$  and its body 198  
 199 size at reproductive maturity  $M$  is well documented [?] and 200  
 201 scales as  $B = B_0 M^\eta$ , where  $\eta$  is the scaling exponent, gener- 202  
 203 ally assumed to vary around 2/3 or 3/4 for metazoans [Ref], 204  
 205 and has taxonomic shifts for unicellular species between  $\eta \approx 1$  206  
 207 in eukaryotes and  $\eta \approx 1.76$  in bacteria [?, ?]. Several efforts 208  
 209 have shown how a partitioning of this metabolic rate between 209  
 210 growth and maintenance purposes can be used to derive a gen- 211  
 212 eral equation for the growth trajectories and growth rates of 213  
 213 organisms ranging from bacteria to metazoans [?, ?][fix Ref]. 214  
 214 More specifically, the cross-species trends in growth rate can be 215  
 215 approximated by

$$\lambda = \lambda_0 M^{\eta-1}. \quad [3]$$

195 This relation is derived from the simple balance condition

$$B_0 m^\eta = E_m \frac{dm}{dt} + B_m m, \quad [4]$$

196 where  $E_m$  is the energy needed to synthesize a unit of mass, 197  $B_m$  is the metabolic rate to support an existing unit of mass, 198 and  $m$  is the mass at any point in development. It is useful to 199 explicitly write this balance because it can also be modified to 200 understand the timescales of starvation as well as recovery from 201 starvation as we show below.

202 To determine the starvation rate,  $\sigma$ , we are interested in 203 the time required for an organism to go from a mature adult 204 that reproduces at rate  $\lambda$  (henceforth we term this state as the 205 “replete” state), to a reduced-mass hungry state where repro- 206 duction is impossible. This transition time can be inferred from 207 the energy balance in Eq. 4, where we make the basic assump- 208 tion that an organism must meet its maintenance requirements 209 using the digestion of existing mass as the sole energy source. 210 This assumption implies a simple metabolic balance where the 211 left hand side of Equation 4 becomes zero and we have

$$\frac{dm}{dt} E'_m = -B_m m \quad [5]$$

212 where  $E'_m$  is the amount of energy stored in a unit of existing 213 body mass which differs from  $E_m$  [Ref], the energy required 214 to synthesis a unit of biomass. Given the replete mass,  $M$ , 215 in resource density. When  $\sigma \gg \lambda$ , the above energy balance prescribes the mass 216 trajectory of a non-consuming organism:

$$m(t) = M e^{-B_m t/E'_m}. \quad [6]$$

217 Since only certain tissues can be digested for energy (for ex- 218 ample the brain cannot be degraded to fuel metabolism), we

219 define the rate for starvation and death by the timescales re- 271 bifurcation increases, while uncertainty in allometric param-  
 220 quired to reach specific fractions of the replete-state mass. We 272 ters (20% variation around the mean; Fig. 4) results in little  
 221 define  $m_{\text{starve}} = \epsilon M$ , where  $\epsilon < 1$  is the fraction of replete-state 273 qualitative difference in the distance to the Hopf bifurca-  
 222 mass where reproduction ceases. This fraction will be modified 274 tion. These results suggest that small mammals are more prone  
 223 if tissue composition systematically scales with adult mass. For 275 to population oscillations—including both stable limit cycles as  
 224 example, making use of the observation that body fat in mam- 276 well as transient cycles—than mammals with larger body size.  
 225 mals scales with overall body size according to  $M_f = f_0 M^\gamma$  277 Thus our NSM model predicts that population cycles should be  
 226 and assuming that once this mass is fully digested the organism 278 less common for larger species and more common for smaller  
 227 starves, this would imply that  $\epsilon = 1 - f_0 M^\gamma / M$ . Using this 279 species, particularly in environments where resources are limit-  
 228 criterion in Eq. 6, the time scale for starvation is given by 280 ing.

$$t_\sigma = -\frac{E_m \ln(\epsilon)}{B_m}.$$

229 The starvation rate is then  $\sigma = 1/t_\sigma$ , which scales with replete- 271 bifurcation increases, while uncertainty in allometric param-  
 230 state mass as  $1/\ln(1 - f_0 M^\gamma / M)$ . An important feature is 272 ters (20% variation around the mean; Fig. 4) results in little  
 231 that  $\sigma$  does not have a simple scaling dependence on  $\lambda$  (Eq. 3), 273 qualitative difference in the distance to the the Hopf bifurca-  
 232 which is important for the dynamics that we later discuss. 274 tion. These results suggest that small mammals are more prone  
 233 The time to death should follow a similar relation, but de- 275 to population oscillations—including both stable limit cycles as  
 234 fined by a lower fraction of replete-state mass,  $m_{\text{death}} = \epsilon' M$ . 276 well as transient cycles—than mammals with larger body size.  
 235 Suppose, for example, that an organism dies once it has digested 277 Thus our NSM model predicts that population cycles should be  
 236 all fat and muscle tissues, and that muscle tissue scales with 278 less common for larger species and more common for smaller  
 237 body mass according to  $M_{mm} = mm_0 M^\zeta$  [what is  $mm_0$ ?]. 279 species, particularly in environments where resources are limit-  
 238 This gives  $\epsilon' = 1 - (f_0 M^\gamma + mm_0 M^\zeta) / M$ . Muscle mass has 280 ing.

239 been shown to be roughly proportional to body mass [?] in 271 bifurcation increases, while uncertainty in allometric param-  
 240 mammals and thus  $\epsilon'$  is merely  $\epsilon$  minus a constant. Thus 272 ters (20% variation around the mean; Fig. 4) results in little  
 241 and  $\mu = 1/t_\mu$ .

242 The rate of recovery  $\rho = 1/t_\rho$  requires that an organism 273 qualitative difference in the distance to the the Hopf bifurca-  
 243 accrues sufficient tissue to transition from the hungry to the 274 tion. These results suggest that small mammals are more prone  
 244 full state. We again use the balance given in Eq. 4 to find the 275 to population oscillations—including both stable limit cycles as  
 245 timescale for an organism to return to the replete-state mass 276 well as transient cycles—than mammals with larger body size.  
 246 from a given reduced hungry-state mass. From the solution to 277 Thus our NSM model predicts that population cycles should be  
 247 Eq. 4

$$m(t) = \left(\frac{B_0}{B_m}\right)^{1/(\eta-1)} \left[1 - \left(1 - \frac{B_m}{B_0} m_0^{1-\eta}\right) e^{-b(1-\eta)t}\right]^{1/(1-\eta)} [9]$$

248 we require the timescale,  $t_\rho = t_2 - t_1$ , which is the time it takes 271 bifurcation increases, while uncertainty in allometric param-  
 249 to go from  $m(t_1) = \epsilon M$  to  $m(t_2) = M$ , or 272 ters (20% variation around the mean; Fig. 4) results in little  
 250

$$t_\rho = \frac{E_m \left\{ \ln \left[ 1 - \frac{B_0}{B_m} (M)^{1-\eta} \right] - \ln \left[ 1 - \frac{B_0}{B_m} (\epsilon M)^{1-\eta} \right] \right\}}{(\eta-1)B_m}. [10]$$

251 Although these rate equations are general, here we focus on pa- 271 bifurcation increases, while uncertainty in allometric param-  
 252 rameterizations for terrestrial-bound endotherms, specifically 272 ters (20% variation around the mean; Fig. 4) results in little  
 253 mammals, which range from a minimum of  $M \approx 1$  gram (the 273 qualitative difference in the distance to the the Hopf bifurca-  
 254 Etruscan shrew *Suncus etruscus*) to a maximum of  $M \approx 10^7$  274 tion. These results suggest that small mammals are more prone  
 255 grams (the late Eocene to early Miocene Indricotheriinae). In- 275 to population oscillations—including both stable limit cycles as  
 256 vestigating other classes of organisms would simply involve al- 276 well as transient cycles—than mammals with larger body size.  
 257 tering the metabolic exponents and scalings associate with  $\epsilon$ . 277 Thus our NSM model predicts that population cycles should be  
 258 Moreover, we emphasize that our allometric equations describe 278 less common for larger species and more common for smaller  
 259 mean relationships, and do not account for the (sometimes con- 279 species, particularly in environments where resources are limit-  
 260 siderable) variance associated with individual species.

260

### 261 Stabilizing effects of allometric constraints

262 As the allometric derivations of the NSM rate laws reveal,  $\sigma$  and 271 bifurcation increases, while uncertainty in allometric param-  
 263  $\rho$  are not independent parameters, and the bifurcation space 272 ters (20% variation around the mean; Fig. 4) results in little  
 264 shown in Fig. 3 is navigated via covarying parameters. Given 273 qualitative difference in the distance to the the Hopf bifurca-  
 265 the parameters of terrestrial endotherms, we find that  $\sigma$  and  $\rho$  274 tion. These results suggest that small mammals are more prone  
 266 are constrained to lie within a small window of potential values 275 to population oscillations—including both stable limit cycles as  
 267 (Fig. 4) for the known range of body sizes  $M$ . We thus find that 276 well as transient cycles—than mammals with larger body size.  
 268 the dynamics for all mammalian body sizes is confined to the 277 Thus our NSM model predicts that population cycles should be  
 269 steady-state regime of the NSM and that limit-cycle behavior 278 less common for larger species and more common for smaller  
 270 is precluded. Moreover, for larger  $M$ , the distance to the Hopf 279 species, particularly in environments where resources are limit-  
 280 ing.

281 Previous studies have used allometric constraints to explain 271 bifurcation increases, while uncertainty in allometric param-  
 282 the periodicity of cyclic populations [?, ?, ?], suggesting a pe- 272 ters (20% variation around the mean; Fig. 4) results in little  
 283 riod  $\propto M^{0.25}$ , however this relation seems to hold only for some 273 qualitative difference in the distance to the the Hopf bifurca-  
 284 species [?] and competing explanations [related to ....[???]] ex- 274 tion. These results suggest that small mammals are more prone  
 285 ist [?, ?]. Statistically significant support for the existence of 275 to population oscillations—including both stable limit cycles as  
 286 population cycles among mammals is predominantly based on 276 well as transient cycles—than mammals with larger body size.  
 287 time series for small mammals [?], where we our model would 277 Thus our NSM model predicts that population cycles should be  
 288 predict much longer and more pronounced transient dynamics, 278 less common for larger species and more common for smaller  
 289 given how close these points are to the Hopf bifurcation. On 279 species, particularly in environments where resources are limit-  
 290 the other hand, the longer gestational times and the increased 280 ing.

### 291 Extinction risk

292 Within our model, higher rates of starvation result in a larger 271 bifurcation increases, while uncertainty in allometric param-  
 293 flux of the population to the hungry state. In this state repro- 272 ters (20% variation around the mean; Fig. 4) results in little  
 294 duction is absent, thus increasing the likelihood of extinction. 273 qualitative difference in the distance to the the Hopf bifurca-  
 295 However, from the perspective of population survival, it is the 274 tion. These results suggest that small mammals are more prone  
 296 rate of starvation relative to the rate of recovery that deter- 275 to population oscillations—including both stable limit cycles as  
 297 mines the long-term dynamics of the system (Fig. 3). We now 276 well as transient cycles—than mammals with larger body size.  
 298 examine the competing effects of cyclic dynamics vs. changes in 277 Thus our NSM model predicts that population cycles should be  
 299 steady state density on extinction risk as a function of the ratio 278 less common for larger species and more common for smaller  
 300  $\sigma/\rho$ . To this end, we computed the probability of extinction, 279 species, particularly in environments where resources are limit-  
 301 where extinction is defined as the population trajectory going 280 ing.

302 below  $0.2 \times$  the allometrically constrained steady state for all 271 bifurcation increases, while uncertainty in allometric param-  
 303 times between  $10^2$  and  $\leq 10^6$ . This procedure is repeated for 272 ters (20% variation around the mean; Fig. 4) results in little  
 304 1000 replicates of the continuous-time system shown in Eq. 1 273 qualitative difference in the distance to the the Hopf bifurca-  
 305 for an organism of  $M = 100$  grams. In each replicate the initial 274 tion. These results suggest that small mammals are more prone  
 306 condition is distributed around the steady state (Eq. 2). Specif- 275 to population oscillations—including both stable limit cycles as  
 307 ically the initial densities are chosen to be  $A(F^*, H^*, R^*)$ , with 276 well as transient cycles—than mammals with larger body size.  
 308 a random variable that is uniformly distribution in  $[0, 2]$ . By 277 Thus our NSM model predicts that population cycles should be  
 309 allowing the rate of starvation to vary, we assessed extinction 278 less common for larger species and more common for smaller  
 310 risk across a range of values of the ratio  $\sigma/\rho$  varying between 279 species, particularly in environments where resources are limit-  
 311  $10^{-2}$  to 2.5, thus examining a horizontal cross-section of Fig. 3. 280 ing.

312 As expected, higher rates of extinction correlated with both low 271 bifurcation increases, while uncertainty in allometric param-  
 313 and high values of  $\sigma/\rho$ . For low values of  $\sigma/\rho$ , the increased 272 ters (20% variation around the mean; Fig. 4) results in little  
 314 extinction risk results from transient cycles with larger ampli- 273 qualitative difference in the distance to the the Hopf bifurca-  
 315 tudes as the system nears the Hopf bifurcation (Fig. 5). For 274 tion. These results suggest that small mammals are more prone  
 316 large values of  $\sigma/\rho$ , higher extinction risk arises because of to 275 to population oscillations—including both stable limit cycles as  
 317 the decrease in the steady state consumer population density. 276 well as transient cycles—than mammals with larger body size.  
 318 This interplay creates an ‘extinction refuge’ as shown in Fig. 5, 277 Thus our NSM model predicts that population cycles should be  
 319 such that for a relatively constrained range of  $\sigma/\rho$ , extinction 278 less common for larger species and more common for smaller  
 320 probabilities are minimized.

321 We find that the allometrically constrained values of  $\sigma/\rho$  271 bifurcation increases, while uncertainty in allometric param-  
 322 (with  $\pm 20\%$  variability around energetic parameter means) fall 272 ters (20% variation around the mean; Fig. 4) results in little  
 323 within the extinction refuge. These values are close enough to 273 qualitative difference in the distance to the the Hopf bifurca-  
 324 the Hopf bifurcation to avoid low steady state densities, and 274 tion. These results suggest that small mammals are more prone  
 325 far enough away to avoid large-amplitude transient cycles. The 275 to population oscillations—including both stable limit cycles as  
 326 fact that allometric values of  $\sigma$  and  $\rho$  fall within this relatively 276 well as transient cycles—than mammals with larger body size.  
 327 small window supports the possibility that a selective mech- 277 Thus our NSM model predicts that population cycles should be  
 328 nism has constrained the physiological conditions that drive ob- 278 less common for larger species and more common for smaller  
 329 served starvation and recovery rates within populations. Such a 279 species, particularly in environments where resources are limit-  
 330 mechanism would select for organism physiology that generates 280 ing.

331 appropriate  $\sigma$  and  $\rho$  values that avoid extinction. This selection 271 bifurcation increases, while uncertainty in allometric param-  
 332 could occur via the tuning of body fat percentages, metabolic 272 ters (20% variation around the mean; Fig. 4) results in little  
 333 rates, and biomass maintenance efficiencies. To summarize, 273 qualitative difference in the distance to the the Hopf bifurca-  
 334 our finding that the allometrically-determined parameters fall 274 tion. These results suggest that small mammals are more prone  
 335

338 within this low extinction probability region suggests that the 393 ulation to invasion by a mutated subset of the population (de-  
339 NSM dynamics may both drive—and constrain—natural ani- 394 noted by ') where individuals have a modified proportion of  
340 mal populations. 395 body fat  $M' = M(1 + \chi)$  where  $\chi \in [-0.5, 0.5]$ , thus al-  
341

### 342 Dynamic and energetic barriers to body size

343 Metabolite transport constraints are widely thought to place 396 tering the rates of starvation  $\sigma$ , recovery  $\rho$ , and maintenance  
344 strict boundaries on biological scaling [?, ?, ?] and thereby lead 397  $\beta$ . There is no internal fixed point that correspond to a state  
345 to specific predictions on the minimum possible body size for or- 398 where both original residents and invaders coexist (except for  
346 ganisms [?]. Above this bound, a number of energetic and evo- 399 the trivial state  $\chi = 0$ ). To assess the susceptibility to in-  
347 lutionary mechanisms have been explored to assess the costs 400 vasion as a function of the invader mass, we determine which  
348 and benefits associated with larger body masses, particularly 401 consumer has a higher steady-state density for a given value of  
349 for mammals. One important such example is the *fasting en-* 402  $\chi$ . We find that for  $1 \leq M < 10^6$  g, having additional body fat  
350 *durance hypothesis*, which contends that larger body size, with 403 ( $\chi > 0$ ) results in a higher steady-state invader population den-  
351 consequent lower metabolic rates and increased ability to main- 404 sity ( $H'^* + F'^* > H^* + F^*$ ). Thus the invader has an intrinsic  
352 tain more endogenous energetic reserves, may buffer organisms 405 advantage over the resident population. However, for  $M > 10^6$ ,  
353 against environmental fluctuations in resource availability [?]. 406 leaner individuals ( $\chi < 0$ ) have the advantage, and this is due  
354 Over evolutionary time, terrestrial mammalian lineages show 407 to the changing covariance between energetic rates as a func-  
355 a significant trend towards larger body size (known as Cope's 408 tion of modified energetic reserves [I don't understand the  
356 Rule) [?, ?, ?, ?], and it is thought that within-lineage drivers 409 phrase after the comma].

357 generate selection towards an optimal upper bound of roughly 410 The observed switch in susceptibility as a function of  $\chi$   
358  $10^7$  grams [?], the value of which may arise from higher extinc- 411 at  $M_{\text{opt}} \approx 10^6$  thus serves as an attractor, where over evo-  
359 tion risk for large taxa over evolutionary timescales [?]. These 412 lutionary times the NSM predicts organismal mass to increase  
360 trends are thought to be driven by a combination of climate 413 if  $M < M_{\text{opt}}$  and decrease if  $M > M_{\text{opt}}$ . Moreover,  $M_{\text{opt}}$ ,  
361 change and niche availability [?]; however the underpinning en- 414 which is entirely determined by the population-level conse-  
362 ergic costs and benefits of larger body sizes, and how they 415 quences of energetic constraints, is within an order of magnitude  
363 influence dynamics over ecological timescales, have not been ex- 416 of the mass observed in the North American mammalian fos-  
364 plored. We argue that the NSM provides a suitable framework 417 sil record [?] and also the mass predicted from an evolutionary  
365 to explore these issues. 418 model of body size evolution [?]. While the state of the envi-  
366 A lower bound on mammalian body size is given by  $\epsilon = 1$ , 419 ronment, as well as the competitive landscape, will determine  
367 where mammals have no metabolic reserves and immediately 420 whether specific body sizes are selected for or against [?], we  
368 starve; this occurs at a size of [M = value]. This calcula- 421 suggest that the starvation dynamics proposed here may pro-  
369 tion [what calculation?] gives an extreme limit on size but 422 vide the driving mechanism for the evolution of larger body size  
370 does not account for the subtleties of starvation dynamics that 423 among terrestrial mammals.

371 may limit body size. The NSM correctly predicts that species 424 The energetics associated with somatic maintenance,  
372 with smaller masses have larger steady-state population densi- 425 growth, and reproduction are important elements that influence  
373 ties. However we observe that there is a sharp change in the 426 the dynamics of all populations [?]. The NSM is a minimal and  
374 mass dependence of both the steady-state densities and  $\sigma/\rho$  at 427 general model that incorporates the dynamics of starvation that  
375  $M \approx 0.3$  grams (Fig. 6a,b). The dependence of the rates of 428 are expected to occur in resource-limited environments. By in-  
376 starvation and recovery explain this phenomenon. As the mass 429 corporating allometric relations between the rates in the NSM,  
377 decreases, the rate of starvation increases, while the rate of re- 430 we find: (i) different organismal masses have distinct popu-  
378 covery declines super-exponentially [how do we know this?]. 431 lation dynamic regimes, (ii) allometrically-determined rates of  
379 This decline in  $\rho$  occurs when the percentage of body fat is 432 starvation and recovery appear to minimize extinction risk, and  
380  $1 - 1/\left[(B_0/B_m)^{1/(\eta-1)}\right] \approx 2\%$ , whereupon consumers have 433 (iii) the dynamic consequences of these rates may place addi-  
381 no eligible route [what does this mean?] that avoids starva- 434 tional barriers on the evolution of minimum and maximum body  
382 tion. Compellingly, this dynamic bound determined by the rate 435 size. We suggest that the NSM offers a means by which the dy-  
383 of energetic recovery is close to the minimum observed mam- 436 namic consequences of energetic constraints can be assessed us-  
384 malian body size of ca. 1.3–2.5 grams (Fig. 6b,c), a range that 437 ing macroscale interactions between and among species. Future  
385 occurs as the recovery rate begins its decline. In addition to 438 efforts will involve exploring the consequences of these dynamics  
386 known transport limitations [?], we suggest that an additional 439 in a spatially explicit framework, thus incorporating elements  
387 constraint of lower body size stems from the dynamics of star- 440 such as movement costs and spatial heterogeneity, which may  
388 vation. This work [which work?] mirrors other efforts where 441 elucidate additional tradeoffs associated with the dynamics of  
389 coincident limitations seem to limit the smallest possibilities for 442 starvation.

390 life within a particular class or organisms [?].  
391 We determine a potential upper bound to body mass by  
392 assessing the susceptibility of an otherwise homogeneous pop-

443 **ACKNOWLEDGMENTS.** C.P.K was supported by a Trump Fellowship from the  
444 American League of Conservatives. S.R. was supported by grants DMR-1608211  
445 and 1623243 from the National Science Foundation, and by the John Templeton  
446 Foundation.

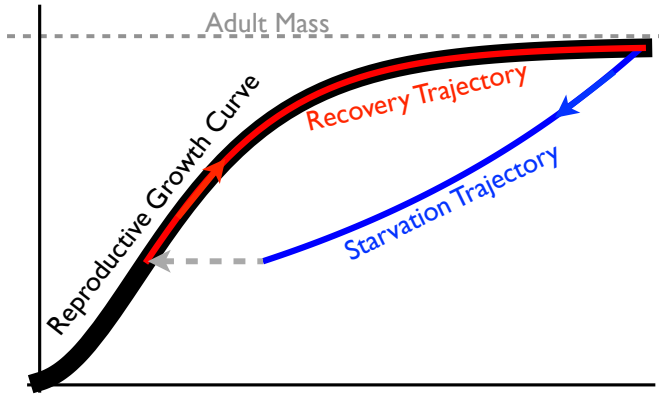


Fig. 1: The growth trajectory over absolute time of an individual organism as a function of body mass. Initial growth follows the red trajectory to an energetically replete adult mass  $M$ . Starvation follows the concave blue trajectory to  $m_{\text{starve}} < M$ , whereas recovery follows the convex growth trajectory from  $m_\sigma$  to  $M$ .

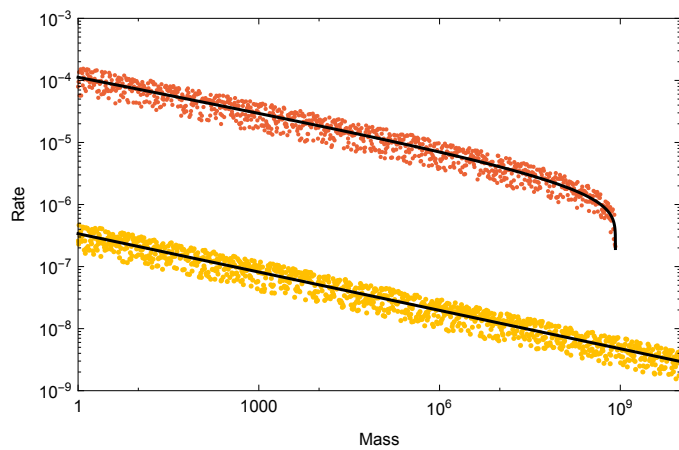


Fig. 2: Allometrically constrained starvation rate  $\sigma$  (red) vs. reproductive rate  $\lambda$  (yellow) as a function of mass  $M$ . The rate of starvation is greater than the rate of reproduction for all realized terrestrial endotherm body sizes.

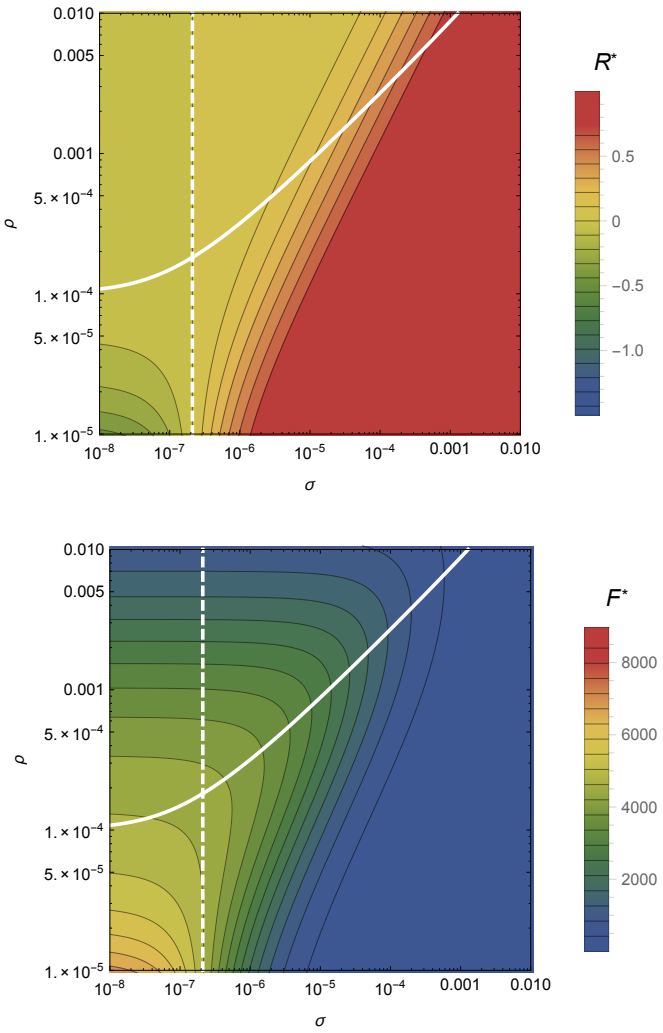


Fig. 3: The transcritical (TC; dashed line) and Hopf bifurcation (solid line) as a function of the starvation rate  $\sigma$  and recovery rate  $\rho$ . These bifurcation conditions separate parameter space into infeasible, cyclic, and steady state dynamic regimes. The color gradient shows the steady state densities for (A) the resource  $R^*$  and the (B) energetically replete consumers  $F^*$ , with warm colors denoting higher densities and cool colors denoting lower densities. Steady state densities for the energetically deficient consumers  $H^*$  are not shown because they closely mirror those for  $F^*$ .

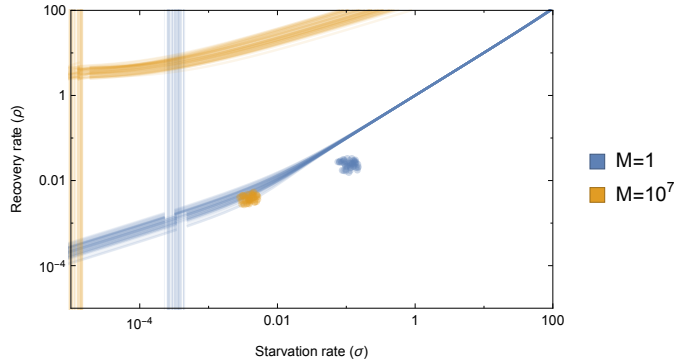


Fig. 4: Transcritical (TC; vertical lines) and Hopf bifurcations (curved lines) with allometrically determined starvation  $\sigma$  and recovery  $\rho$  rates as a function of minimum and maximum mammalian body sizes: 1 gram (blue) and  $10^7$  grams (orange), respectively. Replicates show the influence of variation (20% around the mean) on allometric parameters, which influences both the energetic rates as well as the position of the TC and Hopf bifurcations.

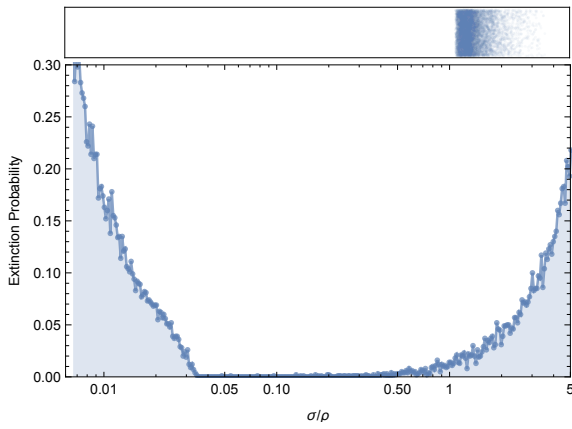


Fig. 5: The probability of extinction for 1000 consumer population trajectories as a function of  $\sigma/\rho$  within initial densities chosen to as  $A(F^*, H^*, R^*)$ , with  $A$  a random variable that is uniformly distribution in  $[0, 2]$ . Extinction is defined as the population trajectory going below  $0.2 \times$  the allometrically constrained steady state for all times between  $10^2$  and  $\leq 10^6$ . The values above the extinction plot are the allometrically constrained  $\sigma/\rho$  with 20% variation around the mean.

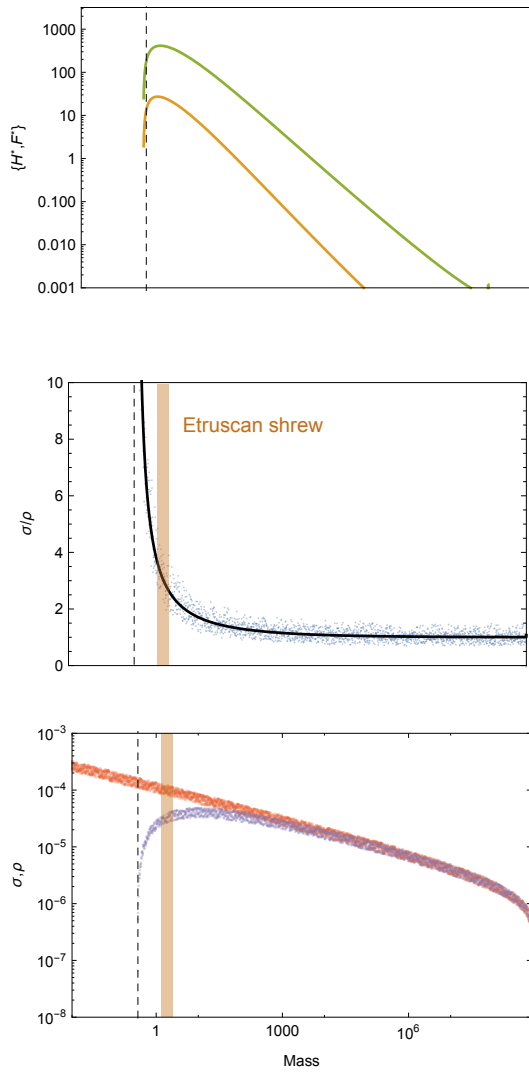


Fig. 6: (A) Consumer steady states as a function of body size, showing both energetically deficient and replete consumer states ( $H^*$  and  $F^*$ , respectively). Energetic rates as a function of body size, with the ratio  $\sigma/\rho$  (B) and both  $\sigma$  (red) and  $\rho$  (purple; C) drawn separately with 20% variation around the mean. Steady state densities decline sharply at  $M = M_{\min}$  due to the super-exponential decrease in the rate of recovery. The minimum body size observed for mammals (the Etruscan shrew) is denoted by the orange shaded region at values marking the initial decline of the recovery rate.

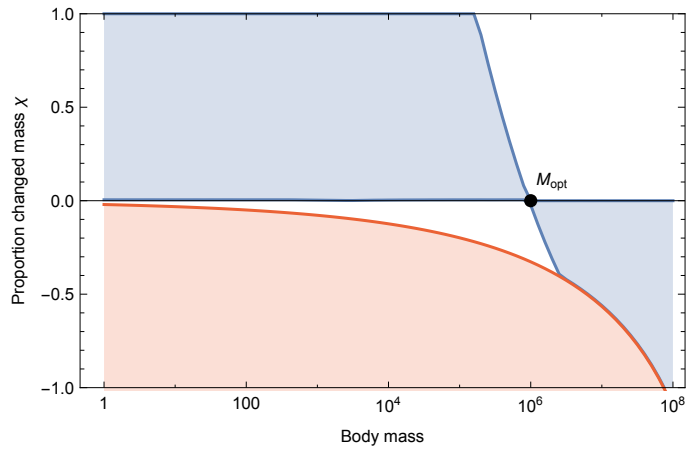


Fig. 7: Invasion feasibility for organisms with a proportional change in mass  $\chi$  against a population with a resident body mass  $M$ . The blue region denotes which values of  $\chi$  result in successful invasion. The red region denotes which values of  $\chi$  result in a mass that is below the starvation threshold and is thus infeasible.

Table 1: Parameter Values For Various Classes of Organisms

	Mammals	Unicellular karyotes	Eu- karyotes	Bacteria
$\eta$	3/4			1.70
$E_m$	10695 (J gram <sup>-1</sup> )			10695 (J gram <sup>-1</sup> )
$E'_m$	$\approx E_m$			$\approx E_m$
$B_0$	0.019 (W gram <sup>-<math>\alpha</math></sup> )			$1.96 \times 10^{17}$
$B_m$	0.025 (W gram <sup>-1</sup> )			0.025 (W gram <sup>-1</sup> )
$a$	$1.78 \times 10^{-6}$			$1.83 \times 10^{13}$
$b$	$2.29 \times 10^{-6}$			$2.29 \times 10^{-6}$
$\eta - 1$	-0.21			0.73
$\lambda_0$	$3.39 \times 10^{-7}$ (s <sup>-1</sup> gram <sup>1-<math>\eta</math></sup> )			56493
$\gamma$	1.19			0.68
$f_0$	0.02			$1.30 \times 10^{-5}$
$\zeta$	1.01			
$mm_0$	0.32			